Published in final edited form as:
*Chem Biol*. 2014 July 17; 21(7): 890–902. doi:10.1016/j.chembiol.2014.06.003.

# A Cell-Permeable Inhibitor to Trap $G\alpha_q$ Proteins in the Empty Pocket Conformation

**Anna-Lena Schmitz**[1], **Ramona Schrage**[2], **Evelyn Gaffal**[3], **Thomas H. Charpentier**[4], **Johannes Wiest**[5], **Georg Hiltensperger**[5], **Julia Morschel**[1], **Stephanie Hennen**[1], **Daniela Häußler**[6], **Velten Horn**[7], **Daniela Wenzel**[8], **Manuel Grundmann**[1], **Katrin M. Büllesbach**[1], **Ralf Schröder**[1], **H. Henning Brewitz**[9], **Johannes Schmidt**[1], **Jesús Gomeza**[1], **Céline Galés**[10], **Bernd K. Fleischmann**[8], **Thomas Tüting**[3], **Diana Imhof**[9], **Daniel Tietze**[7], **Michael Gütschow**[6], **Ulrike Holzgrabe**[5], **John Sondek**[11], **T. Kendall Harden**[4], **Klaus Mohr**[2], and **Evi Kostenis**[1,*]

[1]Molecular, Cellular, and Pharmacobiology Section, Institute of Pharmaceutical Biology, University of Bonn, Nussallee 6, 53115 Bonn, Germany

[2]Pharmacology and Toxicology Section, Institute of Pharmacy, University of Bonn, Gerhard-Domagk-Straße 3, 53121 Bonn, Germany

[3]Department of Dermatology and Allergy, Laboratory of Experimental Dermatology, University of Bonn, Sigmund-Freud-Straße 25, 53105 Bonn, Germany

[4]Department of Pharmacology, School of Medicine, University of North Carolina, Chapel Hill, NC 27599-7365, USA

[5]Pharmaceutical and Medicinal Chemistry, Institute of Pharmacy and Food Chemistry, University of Würzburg, Am Hubland, 97074 Würzburg, Germany

[6]Pharmaceutical Chemistry I, Institute of Pharmacy, University of Bonn, An der Immenburg 4, 53121 Bonn, Germany

[7]Eduard-Zintl-Institute of Inorganic and Physical Chemistry, Technische Universität Darmstadt, Alarich-Weiss-Straße 8, 64287 Darmstadt, Germany

[8]Institute of Physiology I, Life and Brain Center, University of Bonn, Sigmund-Freud-Straße 25, 53105 Bonn, Germany

[9]Pharmaceutical Chemistry I, Institute of Pharmacy, University of Bonn, Brühler Straße 7, 53119 Bonn, Germany

[10]Institut des Maladies Métaboliques et Cardiovasculaires, Institut Nataional de la Santéet de la Recherche Médicale, UniversitéToulouse III Paul Sabatier, 31432 Toulouse, France



*Correspondence: kostenis@uni-bonn.de.

**SUPPLEMENTAL INFORMATION**

Supplemental Information includes Supplemental Experimental Procedures, eight figures, and three tables and can be found with this article online at http://dx.doi.org/10.1016/j.chembiol.2014.06.003.

[11]Department of Pharmacology and Department of Biochemistry and Biophysics and Lineberger Comprehensive Cancer Center, University of North Carolina School of Medicine, Chapel Hill, NC 27599-7365, United States

## SUMMARY

In spite of the crucial role of heterotrimeric G proteins as molecular switches transmitting signals from G protein-coupled receptors, their selective manipulation with small molecule, cell-permeable inhibitors still remains an unmet challenge. Here, we report that the small molecule BIM-46187, previously classified as pan-G protein inhibitor, preferentially silences $G\alpha_q$ signaling in a cellular context-dependent manner. Investigations into its mode of action reveal that BIM traps $G\alpha_q$ in the empty pocket conformation by permitting GDP exit but interdicting GTP entry, a molecular mechanism not yet assigned to any other small molecule Gα inhibitor to date. Our data show that Gα proteins may be “frozen” pharmacologically in an intermediate conformation along their activation pathway and propose a pharmacological strategy to specifically silence Gα subclasses with cell-permeable inhibitors.

## INTRODUCTION

Heterotrimeric αβγ guanine-nucleotide-binding proteins (G proteins) are molecular switches that relay signals from activated G protein-coupled receptors (GPCRs) to (intra)-cellular effector systems such as ion channels or enzymes that, in turn, control production, release, or degradation of second messengers (Wall et al., 1998; Neves et al., 2002; Milligan and Kostenis, 2006; Johnston and Siderovski, 2007; Oldham and Hamm, 2008). These G proteins function by adopting two principal conformational states: an “off state” in which guanosine diphosphate (GDP)-bound Gα is in complex with the Gβγ heterodimer, and an “on state” in which guanosine triphosphate (GTP)-bound Gα is liberated from its Gβγ binding partner. Ligand-activated GPCRs act as guanine nucleotide exchange factors (GEFs) for G proteins that stimulate exchange of GDP for GTP on the Gα subunit (Wall et al., 1998; Johnston and Siderovski, 2007; Oldham and Hamm, 2008; Kimple et al., 2011). Crystal structures have been resolved for both GDP-bound inactive and GTP-bound active conformations and have shed light on the discrete differences of these nucleotide-dependent conformational states (Oldham and Hamm, 2008). Consequently, efforts have been undertaken to develop nucleotide-state-selective inhibitors for both inactive GDP-bound heterotrimers and active GTP-bound Gα or Gβγ dimers (Johnston et al., 2008; Bonacci et al., 2006). Despite enormous advances in understanding structure and function of Gα proteins at a mechanistic level since their discovery, very few small molecule Gα subunit inhibitors with activity in whole cells have been reported to date (Smrcka, 2013). In fact, of the four families of Gα proteins ($G\alpha_{i/o}$, $G\alpha_s$, $G\alpha_{q/11}$, and $G\alpha_{12/13}$) only $G\alpha_{i/o}$ proteins can be specifically inhibited with pertussis toxin (PTX), which has served as an invaluable probe to analyze GPCR signaling mechanisms and $G\alpha_i$-mediated cell responses (Mangmool and Kurose, 2011; Saulière et al., 2012; Ashkenazi et al., 1989; Wong et al., 1991; Itoh et al., 2003). PTX, however, cannot be considered a small molecule but represents a typical A-B toxin using its A protomer to ADP-ribosylate $G\alpha_{i/o}$ protein family members and thereby uncouple receptors from their cognate G proteins (Mangmool and Kurose, 2011; West et al.,

1985). YM-254890, a cyclic depsipeptide isolated from the fermentation broth of *Chromobacterium* sp. QS3666, has recently been shown to specifically silence function of $G\alpha_{q/11}$ proteins, including $G\alpha_{14}$ (Takasaki et al., 2004; Nishimura et al., 2010).

YM-254890 is the only inhibitor for which high-resolution structural information is available to provide the framework for understanding its mechanism of action at the molecular level. A major shortcoming of YM-254890 is that it is not commercially available and, therefore, is only accessible for very few research laboratories worldwide.

In spite of their diverse structures, all inhibitors of Gα function apparently share a common mechanism of action, i.e., bind to Gα subunits to prevent receptor-mediated or intrinsic nucleotide exchange (Smrcka, 2013). This mechanism of action also was proposed for two small molecules, BIM-46174 and BIM-46187, suggested as experimental anticancer drugs (Prévost et al., 2006; Ayoub et al., 2009). BIM-46174 was identified in a differential screening approach as a molecule that inhibits cyclic AMP (cAMP) production in MCF7 cancer cells that were pretreated with the irreversible $G\alpha_s$ activator choleratoxin but not in those pretreated with the direct adenylyl cyclase activator forskolin (Prévost et al., 2006). Such a screening strategy allows identification of compounds that target $G\alpha_s$ proteins but not $G\alpha_s$-sensitive receptors or adenylyl cyclases. Additional mechanistic investigations revealed that both BIM molecules display an intriguing pharmacological phenotype in that they do not only target heterotrimeric G proteins of the $G\alpha_s$ family but also target $G\alpha_{q/11}$, $G\alpha_{i/o}$, and $G\alpha_{12/13}$ proteins, a feature referred to as pan-G protein inhibition (Prévost et al., 2006; Ayoub et al., 2009).

An initial goal of the present study was to take advantage of the pan-G protein inhibitory nature of BIM-46187 to specifically investigate G protein-independent signaling. However, we found that BIM-46187 does not abolish signaling of all Gα subfamilies equally but instead acts in a cellular context-dependent manner, ranging from pan-G protein inhibition to selective $G\alpha_q$ silencing. We identified mammalian human embryonic kidney 293 (HEK293) and Chinese hamster ovary (CHO) cells, two cell lines frequently used to examine signaling of recombinant or endogenous GPCRs, as hosts in which BIM-46187 specifically silences $G\alpha_q$ over $G\alpha_s$, $G\alpha_i$, and $G\alpha_{13}$ proteins. Based on the $G\alpha_q$-specific inhibition, we investigated the molecular mechanism underlying BIM-46187 action. Our results are consistent with the idea that BIM-46187 targets Gα proteins and show that it interferes with agonist function, but not agonist binding to $G\alpha_q$-sensitive GPCRs, by exhibiting a mechanism not yet assigned to any other small molecule Gα inhibitor to date.

## RESULTS

BIM-46174 and the more stable derivative BIM-46187 (Figure 1A, also referred to as BIM-monomer and BIM-dimer, respectively) are two small molecules that interdict signaling of GPCRs by direct binding to and inhibition of α subunits of heterotrimeric G proteins (Prévost et al., 2006; Ayoub et al., 2009). Both molecules are thought to inhibit all Gα subfamilies equally and therefore serve to silence receptor signaling in complex pathologies that involve multiple GPCRs (Smrcka, 2013; Prévost et al., 2006). We wanted to take advantage of the pan-G protein inhibitors to specifically dissect G-protein-dependent versus

G-protein-independent signaling events mediated by cell surface GPCRs. We hypothesized that the free thiol group-containing monomeric BIM should be intrinsically sensitive to oxidation; therefore, we initially investigated stability in aqueous solution ($D_2O$) over time by nuclear magnetic resonance (NMR) spectroscopy (Figure 1B). NMR spectra are clearly indicative of BIM-monomer oxidation in a time-dependent manner: After 48 hr, BIM-monomer is virtually undetectable (Figure 1C). Since the integration area of the signals correlates with the concentration of BIM-monomer, we were able to deduce a half-life of 11.4 hr for this first-order reaction (Figure 1D and Table S1 available online). We reasoned that oxidation of BIM-monomer should depend on the presence of reducing agents and therefore examined stability by NMR in $D_2O$ containing reactive thiols (L-cysteine, glutathione [GSH]), and mercaptoethanol. Indeed, under these conditions, quantitative formation of covalent complexes with selected thiols was observed: BIM-cysteine, BIM-mercaptoethanol, and BIM-dimer (Figure S1). Additionally, we investigated the stability of both BIM-monomer and -dimer during cellular assays by analyzing the cell culture supernatant with liquid chromatography-mass spectrometry. We identified BIM-cysteine, BIM-mercaptoethanol, BIM-dimer, or BIM-monomer, respectively, after 24 hr at 37°C (Figure S2). These data suggest that (1) assessment of biological activity of BIM-monomer should take into account that extracellular BIM-monomer might be entirely converted to BIM-dimer during the assay period, and (2) that both BIM molecules are prone to formation of redox-reversible adducts when thiol-containing components are present. This notion might be particularly relevant when anti-proliferative activity of BIM is assessed, because such assays typically range from many hours to days.

Despite the short duration of assays that assess GPCR activity by quantifying intracellular second messengers and the absence of reducing agents in these assays, we chose the chemically more stable BIM-dimer for further studies. In agreement with the inability of BIM to affect cAMP production in the breast cancer MCF7 and COS7 cell background upon stimulation with the direct adenylyl cyclase mimetic forskolin (Prévost et al., 2006; Ayoub et al., 2009), it did not blunt cAMP synthesis in forskolin-stimulated HEK293 cells (Figure 2A). It is surprising, however, that BIM also was largely ineffective when cAMP production was triggered with prostaglandin $E_1$ ($PGE_1$), a bona fide stimulus of the $G\alpha_s$-linked E prostanoid EP2 and EP4 receptors that are endogenously expressed in this cell system (Figure 2B). Proper functionality of our cAMP assay was ascertained by preincubation of cells in the presence of an EP2/EP4 antagonist, which completely blunted $PGE_1$-mediated cAMP synthesis (Figure S3). Lack of BIM inhibition of $G\alpha_s$-coupled receptor signaling is not due to BIM decomposition during the assay period, because BIM significantly dampened EP2/EP4 receptor signaling in a COS7 cell background (Figure 2C). We therefore reasoned that BIM interferes with G protein signaling in a cell-type-specific manner. Such a pharmacological phenotype would be of relevance for an anticancer agent, particularly if it is applied under the assumption that the entire set of G protein pathways is silenced simultaneously in any cell type.

To explore the consequences of BIM exposure for functionality of the remaining G protein pathways, HEK293 cells were treated with a set of different stimuli for $G\alpha_i$-, $G\alpha_q$-, and $G\alpha_{13}$-linked receptors that are natively or were exogenously expressed in this cell system. It is interesting that preincubation of cells with BIM completely abolished signaling of $G\alpha_q$-

sensitive receptors (Figures 3A–3C) but hardly affected signaling of those that are functionally coupled to $G\alpha_i$ proteins (Figures 3D–3F). Even when cells were preincubated with 100 μM of BIM—the highest applicable concentration—robust $G\alpha_i$ activation was still detected. A similar lack of BIM inhibition was observed when GPCR engagement of $G\alpha_{13}$ signaling was recorded using lysophosphatidylinositol and its target receptor GPR55 in bioluminescence resonance energy transfer (BRET) assays. We recorded a substantial agonist-promoted decrease in BRET in cells coexpressing GPR55 along with the energy donor $G\alpha_{13}$-106*R*Luc8, the energy acceptor $G\gamma_2$-GFP[10], and unlabeled $G\beta_1$. This BRET decrease reflects the separation of the Gα-helical domain from the N terminus of Gγ thereby creating the route for GDP exit and GTP entry (Galés et al., 2006; Saulière et al., 2012). Pretreatment of transfected cells with BIM did not alter GPR55-$G\alpha_{13}$ activation (Figure 3G) but significantly blunted activation-dependent rearrangement of the $G\alpha_q$-$\beta_1\gamma_2$ heterotrimer triggered with carbachol via muscarinic M3 receptors (Figure 3H). These results suggest that the BRET partners used are suitable for examining inhibition of G protein signaling by BIM and that BIM is competent to interdict $G\alpha_q$ but not $G\alpha_{13}$ signaling.

So far, BIM has been applied to a number of different cancer cell lines, such as breast cancer MCF7 and human colorectal cancer HCT8/S11 and HT29, among many others (Ayoub et al., 2009; Prévost et al., 2006). Nonetheless, its utility to silence all G protein signaling pathways in immortalized cell lines that are frequently used for recombinant expression such as HEK293 or CHO is undefined. So far, only COS7 cells have been used as an immortalized host in elegant studies to examine the mechanism of BIM action in great detail (Ayoub et al., 2009). We therefore investigated the influence of BIM on second messenger pathways using CHO cells as an expression system. Again, BIM did not exert pan-G protein inhibitory activity but rather targeted $G\alpha_q$ proteins as evidenced by the clear preference to interdict signaling of the $G\alpha_q$-sensitive muscarinic M1 receptor over $G\alpha_s$-linked prostanoid and $G\alpha_i$-linked serotonin receptors (Figures 4A–4C). A similar preference for inhibition of $G\alpha_q$-signaling was observed when monomeric BIM was applied in analogous second messenger assays, both in CHO (Figures 4D–4F) and HEK cell backgrounds (Figures 4G–4I). From these data, we infer that (1) cellular context-dependent inhibition of $G\alpha_q$ signaling is not related to the inability of the cells to convert dimeric BIM into its reduced counterpart, and hence to different reductive capacities of cells; and (2) dimeric BIM is superior to monomeric BIM for silencing of $G\alpha_q$ signaling, at least in the CHO and HEK cell backgrounds.

We next addressed whether the absence of pan-G protein inhibition may be related to the export of BIM via multidrug transporters. If BIM was a substrate for active outward transport, inhibition of BIM efflux by coadministration of a transport inhibitor should improve its capacity to interdict $G\alpha_q$ signaling. To test this assumption, we pretreated HEK cells, which endogenously express multidrug transporters, with MK571 or elacridar to block efflux protein activity. MK571 inhibits MRP1 and MRP2, two transporters that export hydrophilic molecules and GSH conjugates (Wortelboer et al., 2003; Leyers et al., 2008). Elacridar inhibits P-glycoprotein (P-gp) and breast cancer resistance protein (BCRP), the former preferring hydrophobic and the latter transporting rather diverse and nonconjugated compounds (Ahmed-Belkacem et al., 2005). None of the applied inhibitors rendered $G\alpha_q$

signaling more sensitive toward BIM inhibition (Figure S4). Thus, we conclude that export of BIM via multidrug transporters does not account for cell-type-specific differences in G protein inhibition profiles.

It is interesting to note that BIM displays antiproliferative effects in HEK cells (Prévost et al., 2006) yet only silences $G\alpha_q$ signaling in this cellular background. Furthermore, the effective concentration of BIM to inhibit cellular proliferation is much lower as compared with the concentration required to achieve full silencing of $G\alpha_q$ signaling (compare Prévost et al., 2006 with Figure 3). Such data imply that inhibition of $G\alpha_q$ signaling may be sufficient for blockade of cellular proliferation or that the antiproliferative effects of BIM are unrelated to pan-G protein inhibition. To explore a mechanistic link between G protein inhibition and abrogation of cell growth, we chose to directly compare these parameters in the patient-derived human skin cancer cell line MZ7. BIM exhibited concentration-dependent inhibition of cell growth in MZ7 cells as evidenced by crystal violet staining and determination of cell viability in parallel treatment groups (Figure 5A). A similar reduction of cell growth was obtained on treatment with the DNA-replication inhibitor aphidicolin, which inhibits cell cycle progression at the G1/S phase (Figure 5A). However, aphidicolin-arrested cells resumed cell growth on inhibitor removal as opposed to BIM-treated cells, indicating that BIM likely induces cell death. It is interesting that inhibition of cell growth by BIM was maximal at 10 μM, yet an even greater 10-fold increase of BIM concentration was required to dampen cellular signaling via $G\alpha_i$, $G\alpha_s$, and $G\alpha_q$ pathways (Figures 5B–5D). BIM inhibition of second messenger pathways appears to occur specifically at the level of the G proteins, even at these high concentrations, because prior addition of 100 μM BIM completely blocked endothelin-1, but not thapsigargin-induced $Ca_{2+}$ mobilization (Figure 5B), and because BIM did not lower cAMP production triggered with forskolin (Figure S5) but completely prevented cAMP formation in response to adrenocorticotropic hormone (ACTH), a stimulus for the $G\alpha_s$-sensitive melanocortin 1 (MC1) receptor (Figure 5C). Together, these data indicate that BIM does indeed silence all three second messenger pathways in the cancer MZ7 cell background but at concentrations clearly exceeding those required to inhibit cell growth. This discrepancy may be explained by (1) short (second messenger assays) versus long (cell growth assays) BIM preincubation times; (2) cumulative/cooperative effects of BIM in cell growth assays, where multiple signaling pathways are silenced simultaneously; and/or (3) abrogation of ligand-stimulated signaling (second messenger assays) versus endogenous receptor signaling (cell growth assays).

Context-dependent pharmacology of GPCR ligands is a well-known phenomenon that is widely appreciated. Often, cell-type-specific differences in the relative amount or stoichiometry of signaling components may account for functionally different effects of ligands across cell lines (Kenakin and Christopoulos, 2013). We therefore investigated whether the extent of BIM inhibition may be related to the level of expression of its protein target. To this end, HEK293 cells were enriched with increasing amounts of $G\alpha_q$ proteins using a gene dosing approach (Figures 6A and 6B), and sensitivity of $G\alpha_q$ proteins toward BIM inhibition was examined in assays monitoring inositol monophosphate (IP1) production upon stimulation of endogenous muscarinic M3 receptors with carbachol. Indeed, a clear correlation between BIM inhibition and $G\alpha_q$ expression could be detected: BIM inhibition gradually declined when cellular abundance of $G\alpha_q$ proteins was raised

(Figure 6C). These data imply a link between the expression level of BIM target proteins and the extent of BIM inhibition. We reasoned that the disparate G protein inhibition profiles observed in MZ7 versus HEK293 cells might also be related to cellular Gα abundance and quantified expression of $G\alpha_q$, $G\alpha_s$, and $G\alpha_i$ proteins by immunoblotting in both cell lines. Figures 6D–6F reveal equal expression of $G\alpha_q$ but significantly lower abundance of $G\alpha_s$ in the MZ7 background. These data lend further support to the notion that Gα subunit expression and BIM inhibition might be mechanistically linked. However, enhanced abundance of $G\alpha_i$ proteins in MZ7 cells is incongruent with our hypothesis. Together, these data may help explain the absence of pan-G protein inhibition across diverse cell lines yet also indicate that variation in Gα expression does not exclusively account for cell-type-dependent pharmacology of BIM. Clearly, the mechanistic basis underlying cellular context-dependent inhibition must be ascribed to additional reasons why this apparent paradox exists between $G\alpha_q$ selective inhibition in some cells and pan-G protein inhibition in others.

We were intrigued by the finding that BIM might serve to specifically abrogate $G\alpha_q$ signaling in defined cellular environments and wanted to ascertain that perturbation of $G\alpha_q$-sensitive receptor function is not due to disruption of agonist binding. We chose the carbachol-ligated muscarinic M1 receptor as a model system using radioligand competition assays. Our binding assays in whole CHO-M1 cells clearly revealed that BIM did not impair but rather enhanced carbachol displacement of the radio-antagonist [$^3$H]N-methylscopolamine ([$^3$H]NMS) from M1 receptors (Figure 7A). Hence, inhibition of $G\alpha_q$ signaling by BIM in CHO-M1 cells is due to BIM interference with agonist function but not agonist binding.

BIM has been reported to completely prevent G protein activation in [$^{35}$S]GTPγS binding assays, regardless of whether activation is achieved with a ligand-occupied GPCR, the direct G protein activators mastoparan or $AlF_4^-$, or the $G\alpha_i$ mimetic FUB132 (Prévost et al., 2006; Ayoub et al., 2009). While all of these studies support a direct action of BIM on the Gα protein itself, it has not yet been clarified whether BIM impairs GDP exit or GTP entry. To discriminate between these possibilities, we performed radioligand binding assays on membranes isolated from CHO-M1 cells using the radio-antagonist [$^3$H]NMS. Initial homologous competition experiments indicated that BIM did not compromise antagonist recognition of the M1 receptor (Figure S6). If BIM acted as guanine-nucleotide dissociation inhibitor (GDI), i.e., precluded GDP exit from the nucleotide binding pocket, it would be evident as inhibition of high-affinity agonist binding, a conformational receptor state that is stabilized by the nucleotide-free, empty-pocket G protein (De Lean et al., 1980; Oldham and Hamm, 2008; Rodbell et al., 1971). Note that high-affinity ternary complexes can only be visualized when guanine nucleotides are absent but are short-lived intermediates in intact cells where guanine nucleotides are abundant (Rodbell et al., 1971; Oldham and Hamm, 2008; Seifert et al., 1999; De Lean et al., 1980). We also detected high affinity-binding of carbachol to G-protein-coupled and low-affinity binding to G-protein-uncoupled M1 receptors in [$^3$H]NMS competition binding assays (Figure 7B and Table S2). GTP (1 mM) almost completely converted the high-affinity sites to a low-affinity population because, under these conditions, GDP is rapidly exchanged for GTP and the short-lived empty pocket conformation is no longer detectable (Figure 7B and Table S2). In contrast, high-affinity

agonist binding was indistinguishable in the absence and presence of BIM, suggesting that it does not uncouple receptors from their cognate G proteins (Figure 7C and Table S2). Thus, despite the presence of BIM, stable active-state complexes do form, indicating that BIM uncouples high-affinity agonist binding from agonist function. This mode of action can only be rationalized if BIM permitted GDP exit but precluded GTP entry. To further substantiate the proposed mechanism of action, we measured [$^3$H]GDP dissociation from purified recombinant $G\alpha_q$. Since $G\alpha_q$-bound GDP dissociates very slowly (Chidiac et al., 1999), we took advantage of $(NH_4)_2SO_4$ to accelerate and, therefore, visualize its dissociation. GDP dissociation in the presence of 750 mM$(NH_4)_2SO_4$ was complete within 120 min but, notably, unaffected by the presence of BIM (Figure 7D). These data strongly suggest that BIM does not act as a GDI but permits egress of GDP from the nucleotide binding pocket. BIM, however, does counteract the effect of GTP on high-affinity agonist binding (Figure 7E). Therefore, our results are entirely consistent with the view that BIM inhibits $G\alpha_q$ function by permitting GDP exit but precluding GTP entry, i.e., "freezes" $G\alpha_q$ in the empty pocket conformational intermediate along the activation pathway.

To rationalize this mode of inhibitor action, we conducted docking experiments and all-atom molecular dynamics (MD) simulations to assess the effect of BIM on motions required for nucleotide exchange. Given the absence of mutagenic mapping or structural data, two scenarios were taken into consideration. The first scenario was covalent attachment to cysteine residues that are conserved among all Gα proteins but are not part of the Gα/Gβγ interface (C144 and C330 within $G\alpha_q$). This assumption is based on the notion that BIM, in principle, inhibits all Gα subfamilies but does not impair formation of Gα-Gβγ heterotrimers in vitro (Ayoub et al., 2009). The second scenario was noncovalent binding to an epitope within Gα, as determined through independent molecular docking experiments. Docking results reveal high binding energies and a large overlap in the binding sites for BIM-monomer and -dimer, respectively, at least for the best scoring cluster conformations (Figure S7 and Table S3).

We then subjected the individual Gα-BIM complexes to all-atom MD simulations. We calculated average protein structures and used fluctuations of Cα residues relative to the average structure as a measure of dynamic motion, which is often linked to intrinsic domain motion (Jones et al., 2012). As shown in Figure 7F, fluctuations in GDP-$G\alpha_q$ (indicated by black trace) are greatest in the three switch regions of the Ras-like domain and in the αB–αC loop of the helical domain (please note that the energy donor *R*Luc of our $G\alpha_q$ BRET sensor is inserted into the αB–αC loop). When BIM is covalently bound to Cys330 within $G\alpha_q$ (Figure 7F, red trace), the magnitude of local fluctuations in switch regions II and III and in the αB–αC loop is clearly diminished. This reduction in local mobility aligns well with the impaired helical domain motion that is detected in our BRET experiments (compare with Figure 3H). In contrast, when BIM is linked to Cys144, only switch region II and the αB–αC loop display reduced mobility (Figure S8, blue trace). It is intriguing that we observed even higher reduction in local fluctuations, particularly in switch region III for the best scoring complex conformation of BIM-dimer (Figure 7G, magenta trace, and Figure 7H). No changes in the local fluctuations were recorded for the other complex conformations analyzed with all-atom MD simulations (Figures S8B–S8D). Together, we propose three

potential binding sites for BIM. All of these sites are compatible with the notion that BIM impairs intradomain motion within Gα by compromising local mobility, most likely the conformational changes required for GTP binding in the switch regions, and additionally, the large motion of the helical domain away from the Ras-like domain, a prerequisite for GDP/GTP exchange.

## DISCUSSION

Great therapeutic interest exists for modulation of GPCR-promoted signal transduction. Although most current therapies utilize receptor agonists or antagonists (Rask-Andersen et al., 2011), manipulation of GPCR signaling at steps distal to receptors, such as on the level of heterotrimeric G proteins, is an attractive alternative, particularly for diseases with complex pathologies, involving multiple receptors and signaling pathways (Smrcka, 2013). One example for small molecules interfering with GPCR signaling at the postreceptor level are the imidazopyrazine derivatives BIM-46174 and its more stable derivative BIM-46187 (Figure 1A), each reported to dampen cellular signaling of all four families of heterotrimeric G proteins equally, a property coined pan-G protein inhibition (Prévost et al., 2006; Ayoub et al., 2009). The pan-G protein inhibition may represent an innovative molecular intervention to target oncogenic signaling pathways.

We wanted to take advantage of the pan-G protein inhibitory nature of BIM to study G-protein-independent signaling but made three significant observations: (1) BIM does not silence all G protein subfamilies equally but rather interferes with G protein signaling in a cellular context-dependent manner; (2) BIM may even serve to specifically silence $G\alpha_q$ signaling in defined cellular backgrounds; and (3) BIM inhibits Gαβγ heterotrimer function via interference with nucleotide cycling, using a unique molecular mechanism: precluding GTP entry into rather than GDP exit from the nucleotide binding pocket.

Inhibition of heterotrimeric G proteins may be achieved on the level of the αβγ heterotrimer or on the level of the dissociated subunits. Of the few existing inhibitors for G protein signaling, mechanistic details at the structural level are only available for the $G\alpha_q$-selective YM-254890 (Nishimura et al., 2010). Its binding mode, as elucidated by means of mutagenesis and structural data, provides a plausible mechanism for inhibition of GDP release. A similar mechanism of action has been proposed for suramin, a polysulphonated molecule with a preference for inhibiting $G\alpha_s$ proteins, but this molecule is of limited utility in cell-based assays because it does not cross cell membranes due to its strong negative charge (Smrcka, 2013; Hohenegger et al., 1998). BIM has also been proposed to interfere with the GDP/GTP exchange reaction, but it has not been clarified whether BIM resembles suramin and YM in that it prevents receptor-stimulated GDP release. To address this question, we performed radioligand binding studies under conditions that allow assessment of nucleotide-sensitive binding states of GPCRs. Agonist docking to GPCRs promotes an active receptor state that engages heterotrimeric G proteins and initially triggers GDP release from the Gα subunit (Oldham and Hamm, 2008). Nucleotide-free G proteins, in turn, stabilize the agonist-bound active state of GPCRs. These active-state ternary complexes can only be observed when guanine nucleotides are absent but are transient conformational intermediates in intact cells where GTP and GDP are abundant (Rodbell et al., 1971; De

Lean et al., 1980; Seifert et al., 1999). Herein, we took advantage of the formation of such active-state ternary complexes as indicators for the mechanism of interference of BIM with the nucleotide-bound state of Gα. It is well accepted that high-affinity agonist binding can be disrupted with high concentrations of guanine nucleotides such as GTP because, under these conditions, GDP is rapidly exchanged for GTP and the short-lived empty pocket conformation is no longer detectable. Therefore, agents that act like GTP, i.e., promote the uncoupling of the activated G protein from the receptor, can be identified in radio-ligand binding assays. Similarly, such assays are ideal for identifying molecules that stabilize GDP-bound Gα, i.e., act as guanine nucleotide dissociation inhibitors (GDIs). Both GDIs and G-protein-uncoupling agents share the capacity to convert high-affinity agonist sites into low-affinity agonist sites. BIM has been reported to interdict function of Gαβγ heterotrimers (Prévost et al., 2006; Ayoub et al., 2009). Inhibition of heterotrimer signaling can only be achieved with molecules that preclude nucleotide exchange. Because BIM does not compromise high-affinity agonist binding, it must, consequently, permit GDP exit and occurrence of the nucleotide-free, empty pocket transition state of the G protein. Therefore, lack of perturbance of high-affinity agonist binding by BIM can only be rationalized if BIM interfered with GTP entry. Such a mechanism would be entirely consistent with the ability of BIM to permit [$^3$H]GDP dissociation from purified $G\alpha_q$ proteins (Figure 7D). It also explains why BIM enhances carbachol binding to muscarinic M1 receptors in intact cells (Figure 7A), because a GTP entry inhibitor likely prolongs the lifetime of active-state complexes. This mechanism also rationalizes why BIM is incompetent to completely prevent opening of the nucleotide binding pocket of activated $G\alpha_q$-βγ proteins (Figure 3H) in our BRET assay. In this experimental setup, $G\alpha_q$-*R*Luc is coexpressed with $G\gamma_2$-GFP[10] and responds with negative BRET on agonist stimulation of a $G\alpha_q$-sensitive GPCR. This BRET decrease is indicative of the separation of the Gα-helical domain from the N terminus of Gγ and reliably reflects opening of the nucleotide binding pocket, thereby creating the route for GDP exit and GTP entry (Galés et al., 2006; Saulière et al., 2012). In the presence of receptor antagonists, agonist-mediated BRET decrease can be entirely prevented (Galés et al., 2006; Saulière et al., 2012). Inhibitors of G protein function that act as GDIs, such as pertussis toxin, also completely abolish agonist-mediated BRET in this experimental setting (Galés et al., 2006). BIM, in contrast, significantly diminishes negative BRET in response to agonist stimulation but does not completely abolish opening of the nucleotide binding pocket of $G\alpha_q$. We infer from these BRET data (Figure 3H)—in conjunction with our radioligand binding, docking, and MD simulations, as well as in vitro GDP dissociation studies (Figure 7)—that BIM interdicts Gαβγ heterotrimer function by permitting GDP escape but preventing GTP entry. Thus, BIM can be classified as a $G\alpha_q$-specific GTP entry inhibitor that traps $G\alpha_q$ in the empty pocket conformation, thereby blocking receptor-catalyzed activation of the Gαβγ heterotrimer, a mechanism of action not yet assigned to any other small molecule Gα inhibitor to date.

## SIGNIFICANCE

Exchange of GDP for GTP on the Gα subunit is the key step toward G protein activation and initiation of downstream signaling. Structural, biochemical, and biophysical studies on active and inactive conformations of heterotrimeric G proteins have led to the recognition

that Gα subunits are endowed with numerous clefts amenable for small molecule targeting. However, few Gα inhibitors with activities in cellular systems are available to date. Our study is significant for two reasons: first, we show that two small molecules, BIM-46174 and BIM-46187, previously classified as pan-G protein inhibitors, preferably silence $G\alpha_q$ signaling depending on the cellular background. Although the mechanistic basis underlying these disparate, cell-type-dependent G protein inhibition profiles are not clear, BIM molecules may be exploited as lead structures for generation of Gα protein subfamily selective probes, which would be highly desired to understand the contribution of G protein signaling in physiology and disease. Our study also provides a rationale for the development of small molecule probes interrogating $G\alpha_q$'s molecular and physiological functions and its potential as a therapeutic target.

Second, and more significantly, this study proves that cell-permeable inhibitors for Gα proteins may be developed that "freeze" Gα in its empty pocket conformation, an intermediate conformation along the activation pathway. Such inhibitors enrich the mechanistic portfolio of Gα modulators and may constitute important molecules for cocrystallization with Gα to provide deeper insight into the nucleotide-free conformation of Gα proteins. This knowledge will help to refine our picture on the complex series of conformational transitions from agonist binding to G protein activation—events that underlie a host of cellular responses in hormone and neurotransmitter signaling and, therefore, rank among the most fundamental issues in signal transduction.

## EXPERIMENTAL PROCEDURES

### Cell Culture

HEK293 and COS7 cells were maintained in high glucose Dulbecco's modified Eagle's medium (DMEM) supplemented with 10% (v/v) fetal bovine serum and 1% penicillin/streptomycin mixture at 37°C and 5% $CO_2$ in a humidified atmosphere. For culture of human CRTH2-HEK cells, 0.4 mg/ml G418 (InvivoGen) was added to the medium. Stable human free fatty acid receptor 3 (FFA3) Flp-In T-REx and human free fatty acid receptor 2 (FFA2) Flp-In T-REx cells were cultured in DMEM supplemented with 10% fetal calf serum (FCS), 1% penicillin/streptomycin mixture, 15 μg/ml blasticidin, and 100 μg/ml hygromycin B. Expression from the Flp-In locus was induced by treatment with 1 μg/ml doxycycline for 16–18 hr. HEK293 cells stably coexpressing the human 5-oxoeicosatetraenoic acid receptor (OXE-R) and the promiscuous $G\alpha_{16}$ protein (HEK-OXER-$G\alpha_{16}$ cells) were maintained in DMEM supplemented with 10% FCS, 1% penicillin/streptomycin mixture, 0.25 mg/ml hygromycin B, and 0.4 mg/ml G418.

CHO-K1 cells were cultured in Ham's nutrient mixture F-12 GlutaMAX supplemented with 10% (v/v) FCS and 1% penicillin/streptomycin mixture. CHO-M1 cells were maintained in the same medium additionally supplemented with 0.2 mg/ml G418.

The autologous human melanoma cell line MZ7-MEL was established from a splenic melanoma metastasis in 1988. Cells were cultured in complete RPMI 1640 medium supplemented with 10% FCS (Biochrome), 2 mM L-glutamine (GIBCO), 10 mM

nonessential amino acids (GIBCO), 1 mM HEPES (GIBCO), 20 μM 2-mercaptoethanol, 100 IU/ml penicillin, and 100 μg/ml streptomycin (Invitrogen).

### Transfection

For gene dosing experiments, the calcium phosphate DNA precipitation method was used as described elsewhere (Kostenis et al., 2005). Assays were performed 48 hr after transfection.

### Second Messenger cAMP and IP1 Accumulation Assays

Changes of the intracellular second messengers cAMP and IP1 were quantified with the HTRF-cAMP dynamic kit and the HTRF-IP1 kit, respectively (CisBio International), on a Mithras LB 940 reader (Berthold Technologies) according to the manufacturer's instructions and as described elsewhere in detail (Schröder et al., 2009; Schmidt et al., 2011). If BIM or its solvent were present during the assay, it was preincubated for 2 hr at 37°C.

### Crystal Violet Staining

Human melanoma cell line MZ7-MEL was seeded into 96-well plates ($2 \times 10^4$ per well) in complete RPMI medium. BIM was added to the cells in various concentrations (0.1, 0.3, 1, 3. and 10 μM) along with its vehicle. After 72 hr, cells were washed with PBS and fixed with 4% paraformaldehyde for 5 min. Afterward, cells were stained with 0.05% crystal violet dye for 30 min, rinsed twice with tap water, and thoroughly dried. Staining intensity was measured using the Li-Cor Odysee SA imaging system. Values are expressed as percentage staining intensity ± SEM relative to control.

### Colorimetric XTT Assay

Human melanoma cell line MZ7-MEL was seeded into 96-well plates ($2 \times 10^4$ per well). Solvent control, BIM (0.1, 1, 10 and 100 μM), or the cell cycle inhibitor aphidicolin (1 μg/ml) were added in various concentrations to the cells. After 72 hr, cell viability was measured using the XTT-based Cell Proliferation Kit II (Roche) according to the manufacturer's protocols. Absorption was measured at 405 nm using an ELISA-Reader. Results are expressed as percentage metabolic activity ± SEM relative to control.

### Western Blot

Protein lysates were prepared from native HEK293 and MZ7-MEL cells as well as HEK293 cells transfected with different amounts of hemagglutinin (HA)-tagged $G\alpha_q$ protein. Samples (10 or 20 μg of protein) were dissolved in SDS-PAGE sample buffer, heated at 70°C for 10 min, fractionated on 10% acrylamide gels, and electrically transferred to nitrocellulose membranes. Membranes were blocked with Roti Block (Carl Roth) and then incubated in primary antibody solution: anti-HA (#11583816001, Roche); anti-β-tubulin (#3708-100, BioVision); anti-$G\alpha_{q/11}$ (sc-392), anti-$G\alpha_s$ (sc-823), and anti-$G\alpha_{i3}$ (sc-262, all from Santa Cruz Biotechnology). Bound antibodies were detected with an anti-rabbit horseradish-peroxidase-conjugated secondary antibody (ABIN 102010, antibodies-online), visualized by ECL Prime Western blotting reagent (RPN2232, Amersham), and quantified by densitometry (GelScan V6.0 Software).

### Single Cell $[Ca^{2+}]_i$ Imaging

MZ7-MEL tumor cells were incubated for 2 hr with BIM (100 μM) or its solvent DMSO (1:500) in RPMI medium (20% FCS) at 37°C, and mobilization of $[Ca^{2+}]_i$ was monitored as outlined in detail in Supplemental Experimental Procedures.

### BRET

G protein activation was quantified in HEK293 cells transiently transfected to express GPR55, $G\alpha_{13}$-106*R*Luc8 (human muscarinic receptor M3 and $G\alpha_q$-97*R*Luc8 for $G\alpha_q$ pathway), $G\gamma_2$-GFP$^{10}$, and unlabeled $G\beta_1$. Assays were performed 48 hr after transfection. Cells were detached and resuspended in Hank's balanced salt solution with 20 mM HEPES at a density of $1.06 \times 10^6$ cells per ml. A volume of 170 μl cell suspension was seeded in 96-well microplates and incubated with BIM or buffer for 2 hr. After agonist addition, cells were incubated for 2 min (1 min for carbachol). G protein activation was measured after the addition of *R*Luc substrate DeepBlueC coelenterazine (Gold Biotechnology). To detect BRET, light emission at 400 and 515 nm was measured sequentially using a Mithras LB 940 instrument. The BRET signal (milliBRET ratio) was determined by calculating the ratio of the light emitted by the fluorescence acceptor GFP$^{10}$ (515 nm) and the light emitted by *R*luc (400 nm).

### Other Methods

For synthesis of BIM-monomer and -dimer, remaining experimental procedures, and a more detailed description of the aforementioned procedures, see the Supplemental Information.

### Data Analysis

Results are expressed as mean values ± SEM and were analyzed using Graph-Pad Prism 5.04 (Graph Pad). Half maximal effective concentration ($EC_{50}$) values were determined by nonlinear regression, and comparison between two experimental groups was based on a two-tailed Student t test. The p values were considered as significant (*$p < 0.05$), very significant (**$p < 0.01$), and extremely significant (***$p < 0.001$).

## Supplementary Material

Refer to Web version on PubMed Central for supplementary material.

## ACKNOWLEDGMENTS

We are grateful to Nina Heycke for expert technical assistance. This work was supported by the Danish Council for Independent Research, Technology and Production (grant 09-070364 to E.K.), by Deutsche Forschungsgemeinschaft (DFG) Research Unit 926 (Project SP8 to D.W. and B.K.F.), and by a junior research group of the State of North Rhine Westphalia (D.W.). K.B. is a member of the DFG-funded Research Training Group RTG 1873.

## REFERENCES

Ahmed-Belkacem A, Pozza A, Muñoz-Martínez F, Bates SE, Castanys S, Gamarro F, Di Pietro A, Pérez-Victoria JM. Flavonoid structure-activity studies identify 6-prenylchrysin and tectochrysin as potent and specific inhibitors of breast cancer resistance protein ABCG2. Cancer Res. 2005; 65:4852–4860. [PubMed: 15930306]

Ashkenazi A, Ramachandran J, Capon DJ. Acetylcholine analogue stimulates DNA synthesis in brain-derived cells via specific muscarinic receptor subtypes. Nature. 1989; 340:146–150. [PubMed: 2739737]

Ayoub MA, Damian M, Gespach C, Ferrandis E, Lavergne O, De Wever O, Banères J-L, Pin J-P, Prévost GP. Inhibition of heterotrimeric G protein signaling by a small molecule acting on Galpha subunit. J. Biol. Chem. 2009; 284:29136–29145. [PubMed: 19648112]

Bonacci TM, Mathews JL, Yuan C, Lehmann DM, Malik S, Wu D, Font JL, Bidlack JM, Smrcka AV. Differential targeting of Gbetagamma-subunit signaling with small molecules. Science. 2006; 312:443–446. [PubMed: 16627746]

Chidiac P, Markin VS, Ross EM. Kinetic control of guanine nucleotide binding to soluble Galpha(q). Biochem. Pharmacol. 1999; 58:39–48. [PubMed: 10403517]

De Lean A, Stadel JM, Lefkowitz RJ. A ternary complex model explains the agonist-specific binding properties of the adenylate cyclase-coupled beta-adrenergic receptor. J. Biol. Chem. 1980; 255:7108–7117. [PubMed: 6248546]

Galés C, Van Durm JJJ, Schaak S, Pontier S, Percherancier Y, Audet M, Paris H, Bouvier M. Probing the activation-promoted structural rearrangements in preassembled receptor-G protein complexes. Nat. Struct. Mol. Biol. 2006; 13:778–786. [PubMed: 16906158]

Hohenegger M, Waldhoer M, Beindl W, Böing B, Kreimeyer A, Nickel P, Nanoff C, Freissmuth M. Gsalpha-selective G protein antagonists. Proc. Natl. Acad. Sci. USA. 1998; 95:346–351. [PubMed: 9419378]

Itoh Y, Kawamata Y, Harada M, Kobayashi M, Fujii R, Fukusumi S, Ogi K, Hosoya M, Tanaka Y, Uejima H, et al. Free fatty acids regulate insulin secretion from pancreatic beta cells through GPR40. Nature. 2003; 422:173–176. [PubMed: 12629551]

Johnston CA, Siderovski DP. Receptor-mediated activation of heterotrimeric G-proteins: current structural insights. Mol. Pharmacol. 2007; 72:219–230. [PubMed: 17430994]

Johnston CA, Willard FS, Ramer JK, Blaesius R, Roques CN, Siderovski DP. State-selective binding peptides for heterotrimeric G-protein subunits: novel tools for investigating G-protein signaling dynamics. Comb. Chem. High Throughput Screen. 2008; 11:370–381. [PubMed: 18537558]

Jones JC, Jones AM, Temple BRS, Dohlman HG. Differences in intradomain and interdomain motion confer distinct activation properties to structurally similar Gα proteins. Proc. Natl. Acad. Sci. USA. 2012; 109:7275–7279. [PubMed: 22529365]

Kenakin T, Christopoulos A. Signalling bias in new drug discovery: detection, quantification and therapeutic impact. Nat. Rev. Drug Discov. 2013; 12:205–216. [PubMed: 23411724]

Kimple AJ, Bosch DE, Giguère PM, Siderovski DP. Regulators of G-protein signaling and their Gα substrates: promises and challenges in their use as drug discovery targets. Pharmacol. Rev. 2011; 63:728–749. [PubMed: 21737532]

Kostenis E, Martini L, Ellis J, Waldhoer M, Heydorn A, Rosenkilde MM, Norregaard PK, Jorgensen R, Whistler JL, Milligan G. A highly conserved glycine within linker I and the extreme C terminus of G protein alpha subunits interact cooperatively in switching G protein-coupled receptor-to-effector specificity. J. Pharmacol. Exp. Ther. 2005; 313:78–87. [PubMed: 15615862]

Leyers S, Häcker H-G, Wiendlocha J, Gütschow M, Wiese M. A 4-aminobenzoic acid derivative as novel lead for selective inhibitors of multidrug resistance-associated proteins. Bioorg. Med. Chem. Lett. 2008; 18:4761–4763. [PubMed: 18707884]

Mangmool S, Kurose H. G(i/o) protein-dependent and -independent actions of Pertussis Toxin (PTX). Toxins (Basel). 2011; 3:884–899. [PubMed: 22069745]

Milligan G, Kostenis E. Heterotrimeric G-proteins: a short history. Br. J. Pharmacol. 2006; 147(Suppl. 1):S46–S55. [PubMed: 16402120]

Neves SR, Ram PT, Iyengar R. G protein pathways. Science. 2002; 296:1636–1639. [PubMed: 12040175]

Nishimura A, Kitano K, Takasaki J, Taniguchi M, Mizuno N, Tago K, Hakoshima T, Itoh H. Structural basis for the specific inhibition of heterotrimeric Gq protein by a small molecule. Proc. Natl. Acad. Sci. USA. 2010; 107:13666–13671. [PubMed: 20639466]

Oldham WM, Hamm HE. Heterotrimeric G protein activation by G-protein-coupled receptors. Nat. Rev. Mol. Cell Biol. 2008; 9:60–71. [PubMed: 18043707]

Prévost GP, Lonchampt MO, Holbeck S, Attoub S, Zaharevitz D, Alley M, Wright J, Brezak MC, Coulomb H, Savola A, et al. Anticancer activity of BIM-46174, a new inhibitor of the heterotrimeric Galpha/Gbetagamma protein complex. Cancer Res. 2006; 66:9227–9234. [PubMed: 16982767]

Rask-Andersen M, Almén MS, Schiöth HB. Trends in the exploitation of novel drug targets. Nat. Rev. Drug Discov. 2011; 10:579–590. [PubMed: 21804595]

Rodbell M, Krans HM, Pohl SL, Birnbaumer L. The glucagon-sensitive adenyl cyclase system in plasma membranes of rat liver. IV. Effects of guanylnucleotides on binding of 125I-glucagon. J. Biol. Chem. 1971; 246:1872–1876. [PubMed: 4993962]

Saulière A, Bellot M, Paris H, Denis C, Finana F, Hansen JT, Altié M-F, Seguelas M-H, Pathak A, Hansen JL, et al. Deciphering biased-agonism complexity reveals a new active AT1 receptor entity. Nat. Chem. Biol. 2012; 8:622–630. [PubMed: 22634635]

Schmidt J, Smith NJ, Christiansen E, Tikhonova IG, Grundmann M, Hudson BD, Ward RJ, Drewke C, Milligan G, Kostenis E, Ulven T. Selective orthosteric free fatty acid receptor 2 (FFA2) agonists: identification of the structural and chemical requirements for selective activation of FFA2 versus FFA3. J. Biol. Chem. 2011; 286:10628–10640. [PubMed: 21220428]

Schröder R, Merten N, Mathiesen JM, Martini L, Kruljac-Letunic A, Krop F, Blaukat A, Fang Y, Tran E, Ulven T, et al. The C-terminal tail of CRTH2 is a key molecular determinant that constrains Galphai and downstream signaling cascade activation. J. Biol. Chem. 2009; 284:1324–1336. [PubMed: 19010788]

Seifert R, Gether U, Wenzel-Seifert K, Kobilka BK. Effects of guanine, inosine, and xanthine nucleotides on beta(2)-adrenergic receptor/G(s) interactions: evidence for multiple receptor conformations. Mol. Pharmacol. 1999; 56:348–358. [PubMed: 10419554]

Smrcka AV. Molecular targeting of Gα and Gβγ subunits: a potential approach for cancer therapeutics. Trends Pharmacol. Sci. 2013; 34:290–298. [PubMed: 23557963]

Takasaki J, Saito T, Taniguchi M, Kawasaki T, Moritani Y, Hayashi K, Kobori M. A novel Galphaq/11-selective inhibitor. J. Biol. Chem. 2004; 279:47438–47445. [PubMed: 15339913]

Wall MA, Posner BA, Sprang SR. Structural basis of activity and subunit recognition in G protein heterotrimers. Structure. 1998; 6:1169–1183. [PubMed: 9753695]

West RE Jr, Moss J, Vaughan M, Liu T, Liu TY. Pertussis toxin-catalyzed ADP-ribosylation of transducin. Cysteine 347 is the ADP-ribose acceptor site. J. Biol. Chem. 1985; 260:14428–14430. [PubMed: 3863818]

Wong YH, Federman A, Pace AM, Zachary I, Evans T, Pouysségur J, Bourne HR. Mutant alpha subunits of Gi2 inhibit cyclic AMP accumulation. Nature. 1991; 351:63–65. [PubMed: 1851251]

Wortelboer HM, Usta M, van der Velde AE, Boersma MG, Spenkelink B, van Zanden JJ, Rietjens IMCM, van Bladeren PJ, Cnubben NHP. Interplay between MRP inhibition and metabolism of MRP inhibitors: the case of curcumin. Chem. Res. Toxicol. 2003; 16:1642–1651. [PubMed: 14680379]

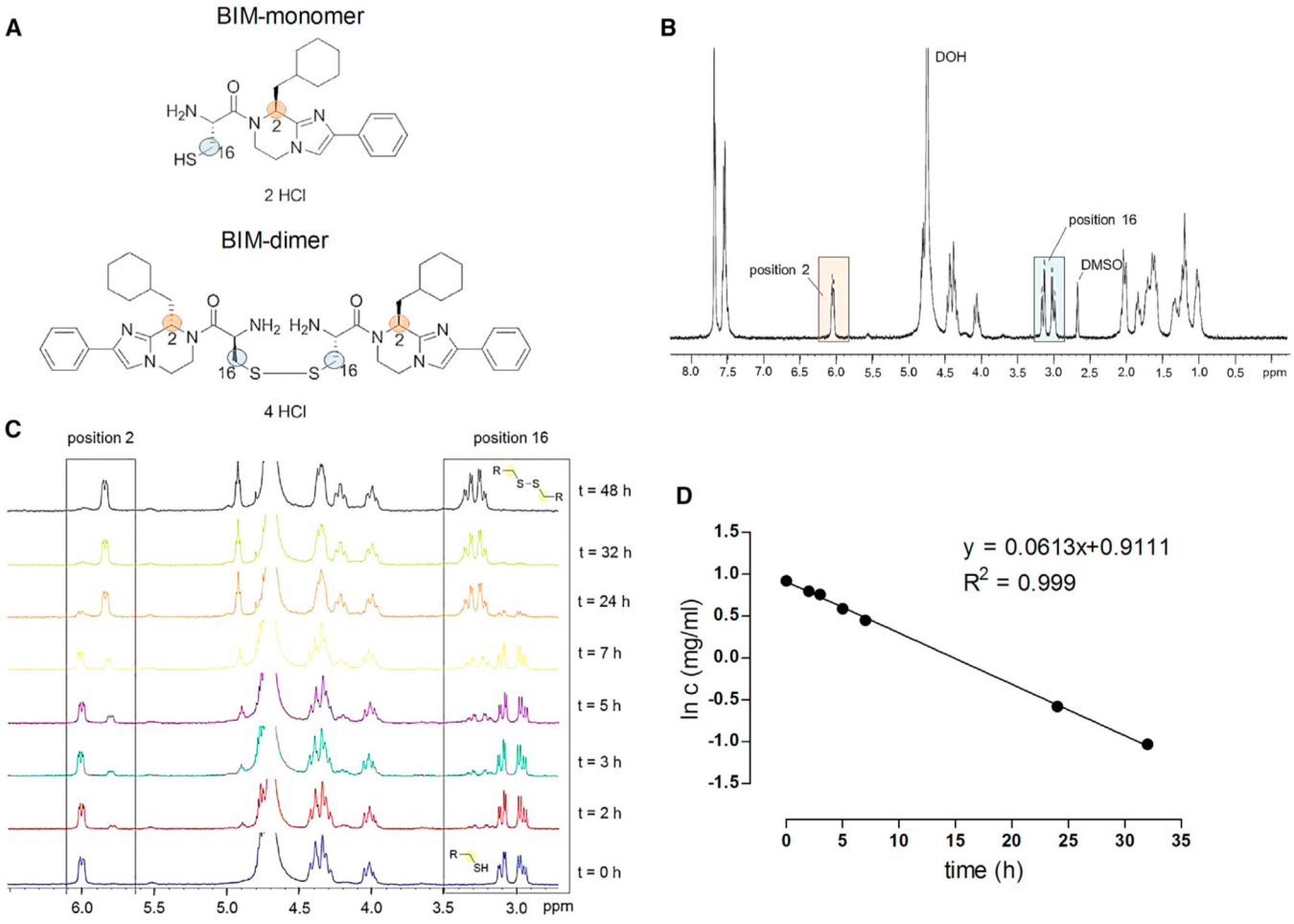


**Figure 1. Structures of BIM-Monomer and BIM-Dimer and Stability in Aqueous Solution, $D_2O$, as Determined by NMR Spectroscopy**

(A) Chemical structures of the BIM-monomer and the BIM-dimer.

(B) $^1H$ NMR of the BIM-monomer at t = 0 hr. The signals at δ = 7.4–7.8 ppm belong to the protons of the aromatic moiety and the imidazole ring. The signal at δ = 6.0 ppm corresponds to the proton in position 2 and the area from δ = 4.0 to 5.0 ppm comprises the protons of position 12, 13 and 15 partially overlayed by the residual solvent (DOH) signal. At about δ = 3 ppm, the diastereotopic methylene protons next to the thiol group resonate (position 16), followed by the DMSO signal and the high-field shifted protons of the cyclohexylmethyl group.

(C) Oxidation of the BIM-monomer over time. The oxidation process can be observed using the protons in position 2 and 16. At t = 0 hr, only the proton signals of the monomer were observed. Within 48 hr, the integration areas of the signals of the monomer protons decrease, while the dimer signals increase until 100% dimer was observed at t = 48 hr. h, hours. R-SH denotes BIM-monomer, and R-S-S-R denotes BIM-dimer.

(D) A diagram of the natural logarithm of the concentration (ln c) of BIM-monomer versus time. Since the integration area of the signals in (C) correlates with the concentration of the BIM-monomer, a half-life of 11.4 hr is calculated for this first-order reaction.

See also Figures S1 and S2 and Table S1.

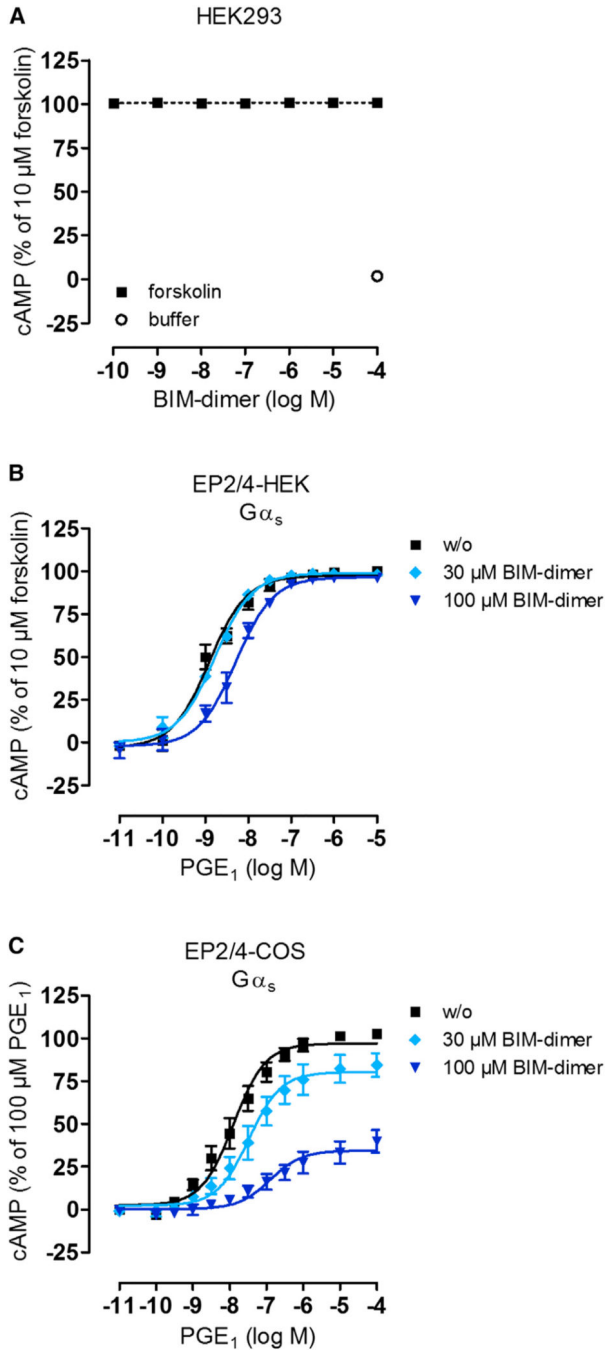


**Figure 2.**

Effects of BIM on Cellular cAMP Levels in an HEK293 and COS7 Cell Background

(A) Increasing concentrations of BIM do not lower forskolin-mediated cAMP production in HEK293 cells.

(B) BIM slightly diminishes cAMP signaling of the $G\alpha_s$-sensitive EP2/EP4 receptors in HEK293 cells. Negative logarithm of $EC_{50}$ ($pEC_{50}$) for $PGE_1$ (without [w/o] BIM) = 8.91 ± 0.07; $pEC_{50}$ for $PGE_1$ (100 µM BIM) = 8.29 ± 0.06.

(C) BIM largely suppresses prostaglandin $E_1$-mediated cAMP production in COS7 cells. Data shown in (A) through (C) are mean values ± SEM of three to ten independent experiments, each performed in triplicate.
See also Figure S3.

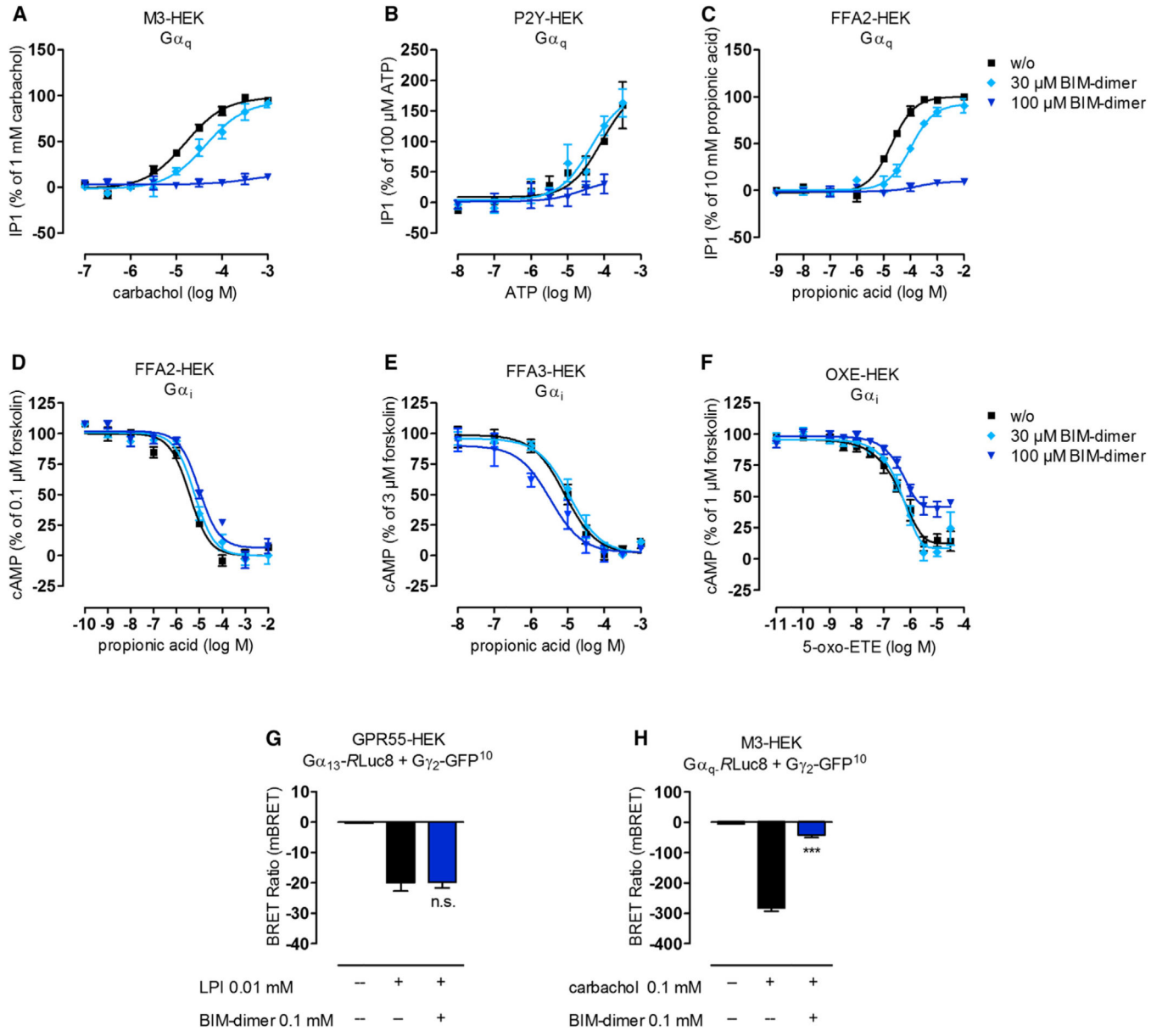


**Figure 3. BIM Interdicts $G\alpha_q$ Signaling but Not $G\alpha_i$ or $G\alpha_{13}$ Signaling in HEK293 Cells**

(A–C) BIM (100 µM) silences $G\alpha_q$ activation induced by stimulation of three $G\alpha_q$-sensitive receptors (muscarinic M3, P2Y, and FFA2) with their cognate agonists carbachol, ATP, and propionic acid, respectively. w/o, without.

(D–F) BIM (100 µM) hardly affects productive $G\alpha_i$ interaction of FFA2 and FFA3, as well as OXE-R.

(G and H) BIM does not block molecular rearrangement of activated $G\alpha_{13}$ (G) but efficiently dampens activation of the $G\alpha_q$-BRET biosensor (H). Opening of the nucleotide binding pocket is detected as BRET decrease after receptor activation in HEK293 cells transfected to express $G\alpha_{13}$-106*R*Luc8 + $G\gamma_2$-GFP$^{10}$ + unlabeled $G\beta_1$ (G) or $G\alpha_q$-97*R*Luc8 + $G\gamma_2$-GFP$^{10}$ + unlabeled $G\beta_1$ (H). ***$p < 0.001$; n.s., not significant.

The means ± SEM in (A) through (F) or + SEM in (G) and (H) of three to six independent experiments, each conducted in triplicate, are shown.

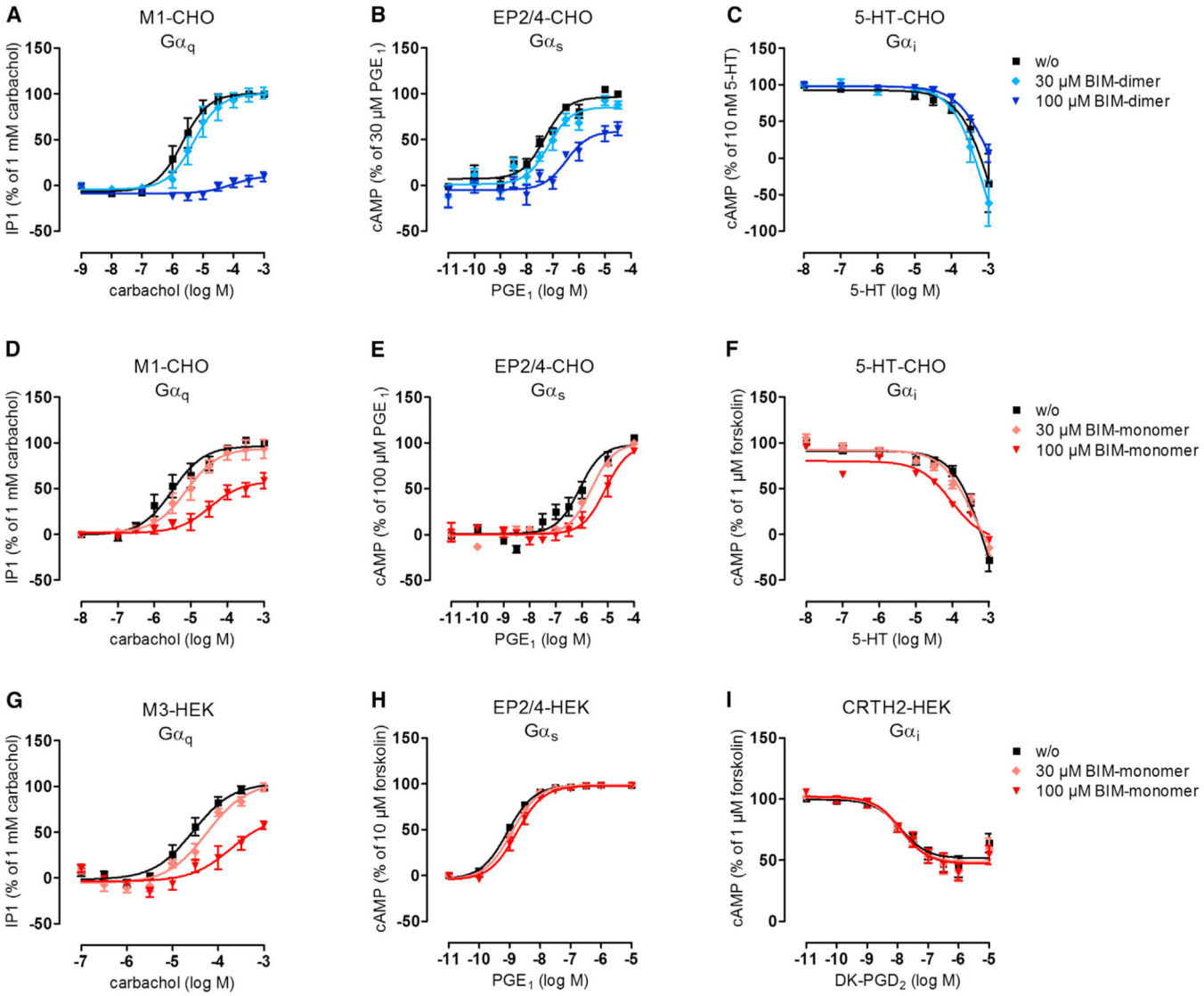


**Figure 4. Monomeric and Dimeric BIM Preferentially Silence $G\alpha_q$ Signaling in a CHO and HEK293 Cell Background**

(A–C) Dimeric BIM almost completely blunts $G\alpha_q$ signaling over $G\alpha_s$ and $G\alpha_i$ signaling in CHO cells transfected to express the muscarinic M1 receptor (A) or endogenously expressing $G\alpha_s$-linked EP2/EP4 receptors (B) and the $G\alpha_i$-sensitive serotonin 5-HT receptors (C).

(D–F) Monomeric BIM resembles dimeric BIM in its ability to preferentially silence $G\alpha_q$ signaling of the muscarinic M1 receptor (D) over $G\alpha_s$ signaling of EP2/EP4 receptors (E) or $G\alpha_i$ signaling of serotonin 5-HT receptors (F) in a CHO cell background yet displays reduced potency and efficacy.

(G–I) Monomeric BIM partially diminishes $G\alpha_q$ activation of the muscarinic M3 receptor in HEK293 cells (G) but does not dampen signaling mediated via $G\alpha_s$-sensitive EP2/EP4 receptors (H) or $G\alpha_i$-sensitive CRTH2 receptors (I). Means ± SEM of at least three experiments, each conducted in triplicate, are shown.

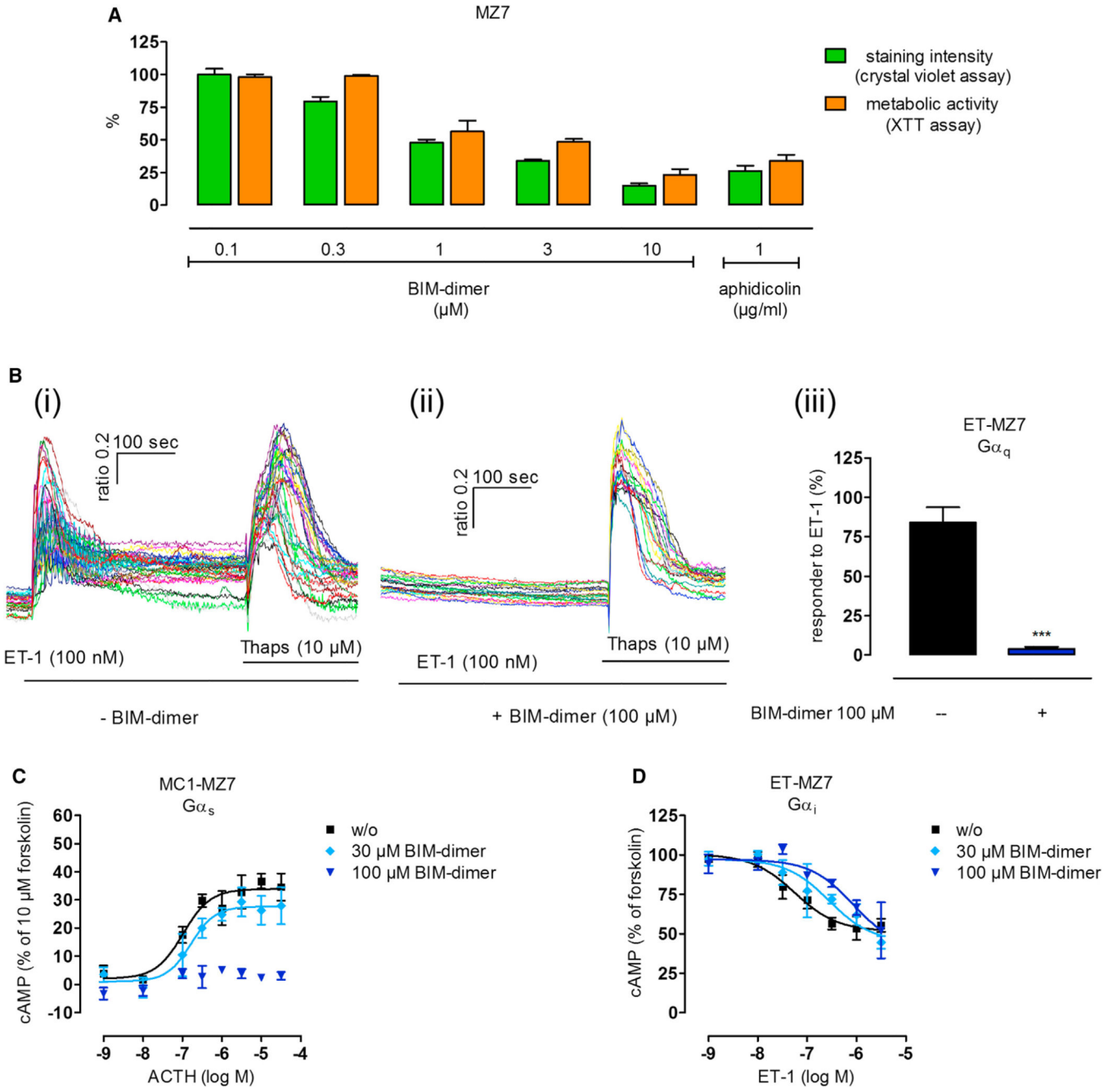


**Figure 5. BIM Inhibits Cell Growth and Second Messenger Production in the Patient-Derived MZ7 Cancer Cell Background**

(A) MZ7 cancer cells were exposed to the indicated concentrations of BIM or the cell cycle inhibitor aphidicolin for 72 hr and cell proliferation was assessed by crystal violet staining (green bars). In parallel treatment groups cell viability was measured using the XTT-based cell viability kit (orange bars), means + SEM, n = 3.

(B) In (i), untreated MZ7 cells respond to both the $G\alpha_q$–stimulus endothelin-1 (ET-1) and thapsigargin (Thaps). (ii) BIM completely blunts $Ca^{2+}$ mobilization triggered with ET-1 but does not impair thapsigargin-induced release of $Ca^{2+}$ from the endoplasmic reticulum. (iii)

Quantification of $Ca^{2+}$ traces in the absence and presence of BIM in single cells. Data in (i) and (ii) show representative traces; data in (iii) are means + SEM of n = 159 cells. sec, seconds. ***$p < 0.001$.

(C) At a concentration of 100 μM, BIM silences $G\alpha_s$-mediated cAMP production induced via ACTH and its cognate $G\alpha_s$-linked MC1 receptor.

(D) BIM diminishes $G\alpha_i$ coupling of endogenous ET-1 receptors. Data shown in (C) and (D) are means ± SEM of three to ten independent experiments, each conducted in triplicate. See also Figure S5.

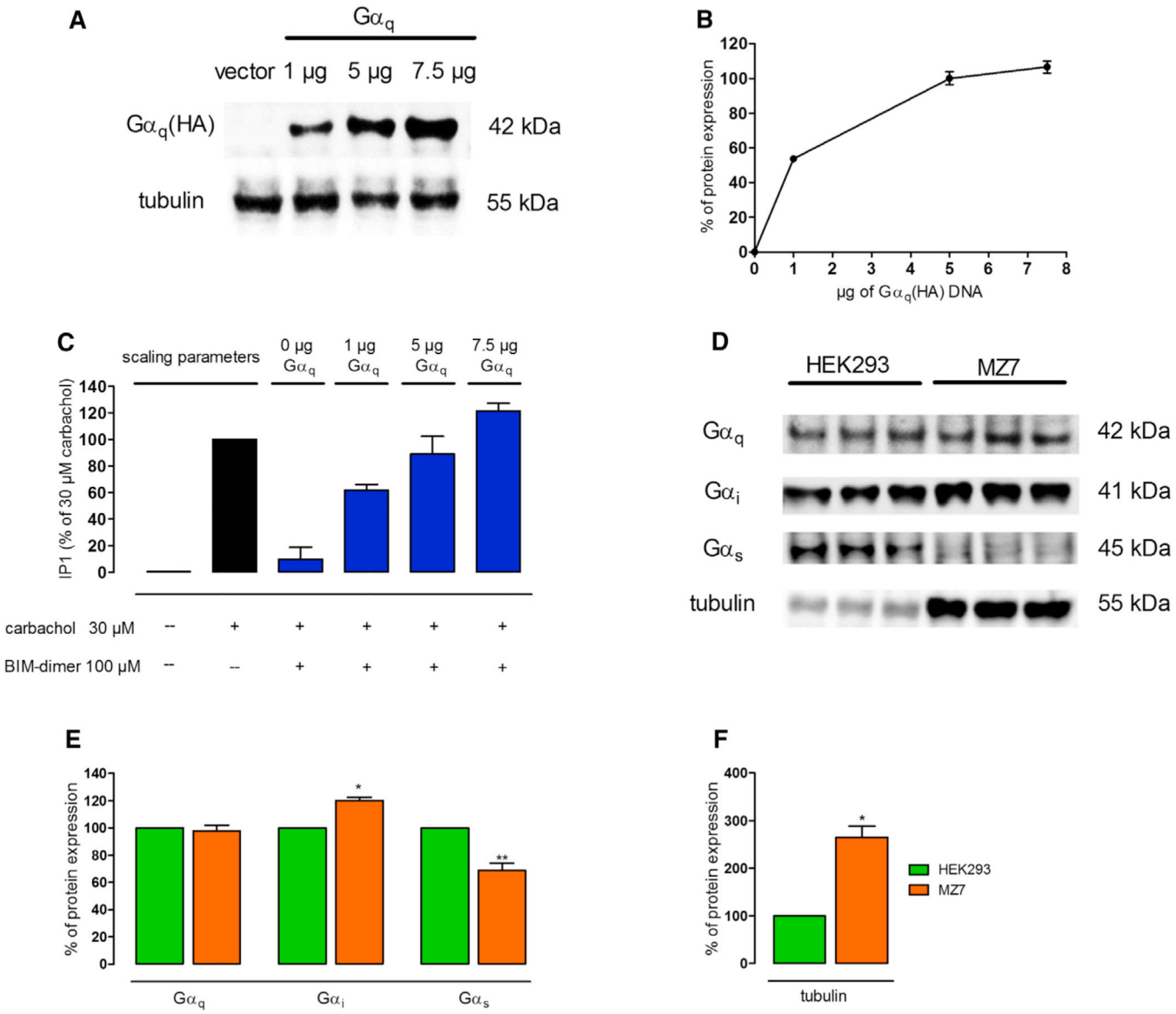


**Figure 6. Mechanistic Link between Sensitivity toward BIM Inhibition and Cellular Abundance of BIM Target Proteins**

(A) Immunoblot detection of HEK293 lysates prepared after transfection with the indicated amounts of $G\alpha_q$ plasmid complementary DNA harboring an internal HA-epitope tag. Membranes were reprobed for tubulin to ensure equal sample loading and transfer. Shown is one representative of four independent experiments.

(B) Densitometric analysis of the immunoblot experiments depicted in (A). Means ± SEM of four individual experiments are shown.

(C) Enrichment of HEK293 cells with the indicated amounts of $G\alpha_q$ proteins is inversely related to BIM inhibition of $G\alpha_q$ signaling (means ± SEM, n = 4).

(D) Immunoblot detection of lysates prepared from native HEK293 and MZ7 cells. Membranes were initially probed for $G\alpha_q$, $G\alpha_i$, and $G\alpha_s$ proteins and then reprobed for

tubulin to ensure equal sample loading and transfer. Shown is one representative of three independent experiments.

(E and F) Densitometric analysis of the immunoblot experiments depicted in (D); means + SEM, n = 3.

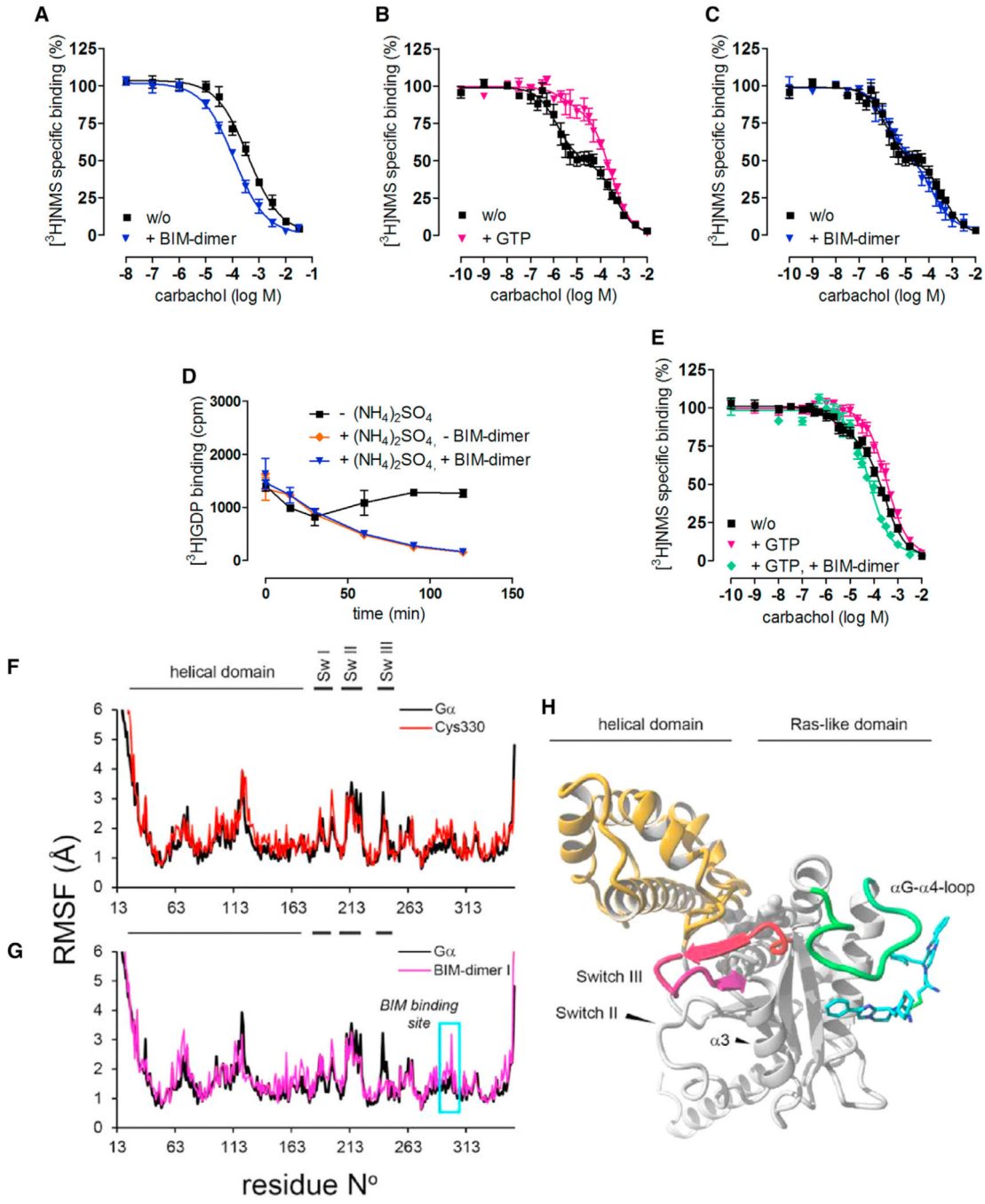


**Figure 7. Effect of BIM on Carbachol Recognition of theM1 Muscarinic Receptor in Radioligand Competition Binding Assays and on [$^3$H]GDP Dissociation from Purified G$\alpha_q$**

(A) BIM (100 μM) enhances carbachol affinity to muscarinic M1 receptors labeled with the radio-antagonist [$^3$H]NMS in whole CHO-M1 cells: $pKI_{(control)}$ = 3.61 ± 0.08, (n = 6); $pKI_{(BIM)}$ = 4.09 ± 0.09, n = 3, $p < 0.05$. w/o, without.

(B) In membrane preparations from CHO-M1 cells, carbachol competes for [$^3$H]NMS sites with high and low affinity. In the presence of 1 mM GTP, 51% of the high-affinity sites were converted to low-affinity sites.

(C) BIM (100 μM) does not impair formation of high-affinity agonist complexes in CHO-M1 membranes.

(D) BIM (100 μM) does not impair [$^3$H]GDP dissociation from purified recombinant $G\alpha_q$. [$^3$H]GDP was preloaded on $G\alpha_q$ for 18 hr before dissociation was visualized in the presence of 750 mM $(NH_4)_2SO_4$.

(E) BIM counteracts the effect of GTP on high-affinity agonist binding in membrane preparations from CHO-M1 cells. In the absence of GTP, 20% of receptors resumed the high-affinity state that was reversed entirely in the presence of GTP, the effect of which was counteracted by BIM. Data in (A) through (E) are means ± SEM of three to four independent experiments, each conducted at least in duplicate.

(F and G) Root-mean-square-fluctuations (RMSF) as a function of their residue number for the indicated simulation. (F) Simulation of GDP-$G\alpha_q$ (black trace), BIM covalently bound to GDP-$G\alpha_q$ (red trace). (G) Simulation of GDP-$G\alpha_q$ (black trace), BIM-dimer complex conformation I (BIM-GDP-$G\alpha_q$, magenta trace). The BIM-dimer binding site encompassing residues 292–311 (αG-α4 loop and α4 helix) is boxed in light blue.

(H) BIM-dimer complex conformation I after 10 ns of MD simulation.

See also Figures S6–S8 and Table S2.